CHAPTER-7

Study of bioactivity of ZnO substituted 45S5 glass after Polarization

7.1 Introduction

The bioactive 45S5 glass is described by its molar composition of 46.1% SiO_2, 26.9% CaO, 24.4% Na_2O, and 2.6% P_2O_5. The origin of the 45S5 glass invention was established by the study of Hench in 1969 [1]. The main benefit of this bioactive glass is its ability to produce a layer consisting of amorphous calcium phosphate [2]. The speed at which the layer forms is considered a significant factor in determining the bioactivity of bioglass, and the synthetic reproduction of the characteristics of this layer has a resemblance to the mineral component found in bone [3]. Hench proposed a relationship between the implant surface attached to tissues, denoted as Ib, and the corresponding time, t0.55b, which represents the point at which more than fifty per cent of the implant surface has been successfully linked to tissues. This relationship is expressed as Ib = 100/t0.55b. The parameter t0.55b is used to ascertain the level of bioactivity shown by a certain implant material [2]. Scholars have recently concentrated on creating biomaterials to enhance biological integration among bioactive implants and the surrounding tissues. Several approaches have been explored to enhance the biological fixation process and increase bioactivity. Many researchers have investigated the effects of an ion substitution and differences in the composition of chemicals on the qualities of biologically active glass, including its ability to deposit hydroxyapatite [4–23]. Some investigations examined the relationship between electrical properties and hydroxyl apatite formation. Furthermore, cellular compatibility, hemocompatibility, and antibacterial properties are investigated [24-26]. Various polling techniques were used to enhance the bioactive properties of materials, including chemical durability, tensile strength, optical non-linearity, and bioactivity [27-28]. One of the most effective techniques for thermal polarization is the thermally induced polarization approach, as described in reference [29]. In this experimental procedure, the specimen underwent the application of a direct current voltage denoted as Vp for a specific time interval referred to as tp while being maintained at a temperature denoted as

Tp [30-31]. The experimental design is structured where voltage application induces the reorientation of the dipolar unit and the migration of the mobile charge carrier [32]. Yamashita [33] revealed the influence of negatively charged surfaces on bioactivity. This was shown by the rapid development of a calcium phosphate film inside the layers of the acquired sample, which exhibited interaction with SBF solution. Obata et al. [34] noticed a change in osteobonding and bone growth on the polarized hydroxyapatite (HA) surface due to the control over ion movement and the establishment of a constant charge on the upper surface layer of the various materials in an *in-vitro* setting. Ferroelectric materials have garnered considerable focus in the area of biomedicine because of their ability to attract different ions. In Nuttapon [28], authors examined the impact of incorporating bioactive ferroelectric composite $Ba_{0.92}Ca_{0.08}Zr_{0.05}Ti_{0.95}O_3$ (BCZT) into 45S5 glass material. The findings revealed that the incorporation of BCZT material not only enhances the dielectric properties of composites but also augments the bioactive properties of the 45S5 glass composite. Zinc is a vital and beneficial component found throughout the human body. Zinc has a diverse range of roles in relation to the immune system, cell division, fertility, and overall development and maintenance of the human body despite its presence at relatively low concentrations. Research has shown that zinc plays a crucial role in many physiological processes, including the organization, mineralization, development, and maintenance of robust skeletal structures [22]. Zinc-deficient bones are prone to osteoporosis, a chronic bone condition in which bone strength is considerably weakened, which has influenced the whole population, particularly older women and individuals, for decades. It serves as both a nourishment for the body and a treatment to prevent various health problems. Zinc has several roles related to the immune system, cell division, fertility, and body development and maintenance. Its deficiency is connected with brain structural malformation, delayed cerebral development, growth stunting, sexual inadequacy and neuropsychological disorders in children. Previous studies have mostly

emphasized the use of zinc in combination with 45S5 bioactive glass since zinc has appealing properties that make it a favourable choice. After the identification of the influence of altering the chemical configuration *in-vitro* bioactive property, the ZNBG samples were subjected to electrical poling. The research aims to evaluate the effect of substituting ZnO for bioactive glass on the bioactive properties of the material. The proposed technique first involves comparing all unpoled samples and then expanding the analysis to include comparisons involving the poled samples. This study will lead to the utilization or exploration of other high K dielectric materials to enhance the bioactivity of materials.

7.2 Materials and Methods

7.2.1 Glass samples synthesis:

ZBG, a bioactive glass, was manufactured using the standard melting procedure, whereby zinc oxide was employed as a replacement material. The first iteration of bioglass, referred to as 45S5, has a molar composition of 46.1% SiO_2, 26.9% CaO, 24.4% Na_2O, and 2.6% P_2O_5. In future iterations, zinc oxide was used as a substitute for Na_2O, with mole percentages ranging from 0% to 3% in increments of 0.5%. The sources of SiO_2, Na_2O, CaO, P_2O_5, and ZnO in the fabrication of ZNBG samples were fine granular quartz (AR grade washed and calcined), sodium carbonate (Na_2CO_3), calcium carbonate ($CaCO_3$), ammonium dihydrogen orthophosphate ($NH_4H_2PO_4$), and zinc oxide (ZnO). Here to make SiO_2 the high surface area quartz powder was used in the study. The mentioned components were carefully calculated and combined in a porcelain mortar and pestle in accordance with the anticipated ratios. Following this, the previously described constituents were subjected to a thermal transformation, whereby they were heated to 1400°C inside an alumina crucible and kept hold at this temperature for a period of two hours. In order to obtain particle sizes smaller than 100 μm, the molten bioglass was subjected to crushing and grinding procedures.

The mole % configurations of the bioactive ZNBG glass samples are included in Table **7.1**.

Table 7.1 Mole % composition of ZBG bioactive glass samples.

Sample code	**SiO_2**	**Na_2O**	**CaO**	**P_2O_5**	**ZnO**
ZBG0	46.1	24.4	26.9	2.6	0
ZBG1	46.1	23.4	26.9	2.6	1
ZBG2	46.1	22.9	26.9	2.6	1.5
ZBG3	46.1	22.4	26.9	2.6	2.0
ZBG4	46.1	21.9	26.9	2.6	2.5
ZBG5	46.1	21.4	26.9	2.6	3.0

7.2.2 Testing and Characterization

7.2.2.1 DTA: Differential thermal analysis (Perkin Elmer Diamond, USA) was used on the sample in order to establish the temperature at which glass crystallizes and nucleates. Alumina was used as a benchmark while the pure bioactive glass sample was heated in a furnace with an argon atmosphere from 35°C to 1000°C at a rate of 7°C/min.

7.2.2.2 XRD: The technique of X-ray diffraction was used on an instrument named XRD RIGAKU-Miniflex II diffractometer from 2 theta angles in the range of 20 to 80° having step size = 0.02° along with step duration = 2 seconds utilizing CuK radiations to identify the phases contained in samples [21]. By referring to the standard XRD dataset of the bio-active glass sample represented by JCPDS, the phase research of unpolarized and polarized materials before and after submersing in SBF solution was carried out.

7.2.2.3 FTIR: Infrared spectroscopy using Fourier transform, (FTIR; Shimadzu-8400S, Japan) was employed in the 400-1400 cm-1 region to examine the functional group found in samples.

7.2.2.4 SEM-EDS: To examine the physical characteristics and chemical content of ZBG samples, both prior to and after immersion in SBF solution, the methods of Energy Dispersion Spectroscopy (EDS) and Scanning Electron Microscopy (SEM) were used using the Inspect 50

FEI instrument. The gold coating was applied to pellets measuring approximately 1 mm in height and 10 mm in diameter before conducting EDS and SEM analysis.

7.2.2.5 AFM: Atomic force microscopy (NT-MDT equipment) was used to evaluate the degraded surface morphologies at a scanning rate of 2μm/s.

7.2.3 *In-vitro* analysis (Biological Characterization):

Kokubo et al. [27] developed a mixture solution called simulated bodily fluid (SBF). This solution has been the most common way to test the biological activity of materials *in-vitro* under conditions similar to those found in vivo. The ionic composition of SBF closely resembles that of human blood plasma. The procedure described by [27] was used in order to generate the simulated bodily fluid (SBF). The formation of the layer of HCA on the surface of bioactive glass by the use of SBF solution is crucial for promoting osteoproduction and facilitating bone formation. The ZBG samples, which were subjected to electro-thermal poling, were categorized as "P-surface" and "N-surface". These samples were immersed in the ratio of 1:100 corresponding sample to SBF solution and then contained in a sterile polypropylene vessel for a duration of 15 days at 37.4ºC temperature in the incubator. The formation of the crystalline HCA layer on samples surface after submersing them in SBF solution was used as an indicator for assessing the bioactivity in an *in-vitro* setting. This evaluation was conducted utilizing XRD, FTIR, SEM-EDS and atomic force microscopy (AFM).

7.2.4 AC conductivity and Dielectric analysis:

An ohmic contact was created by applying conductive silver paint to the surface and the inside of sintered and polished pellets. To achieve accurate compliance with the application of the silver paint, the samples were allowed to dry at 100°C in an oven for 20 minutes after painting. An Impedance Analyzer (Agilent Technologies) was used to measure the room temperature ac conductivity (σ) and dielectric constant (εr) across the frequency ranging from

100Hz to 1MHz. The following equations were used to analyze the dielectric constant (ε_r) and ac conductivity (σ).

$$\boldsymbol{\varepsilon_r = \frac{Ct}{A\varepsilon_0}} \quad \text{..... (7.1)}$$

$$\boldsymbol{\sigma = \omega\varepsilon_0\varepsilon_r \tan\delta} \quad \text{..... (7.2)}$$

Here, C is capacitance, t is thickness, A is the area of the bioglass samples, and ε_0 is the permittivity of free space. In ac conductivity determination, tanδ is dielectric loss, and $\omega=2\pi f$ is the angular frequency [35-36].

7.2.5 Electrical Polarization:

To investigate the influence of electrical polarization on the production ability of hydroxy carbonate apatite in ZnO substituted 45S5 bioactive glasses, the samples were polarized at 500ºC in the connected field of 10KV/cm for 1 hour. Powders were compressed for two minutes at a pressure of 11 tons, with a cylindrical form and having dimensions of 1 mm in height and 10 mm in diameter. Following that, pellets were heated in the furnace for 3 hours up to 500 ºC at a rate of 5 ºC/min and cooled in the furnace. The polarization temperature was selected on the fact that at 500ºC, the bioglass shows maximum conductivity [37-38]. To prevent the polarization from relaxing, the associated field was preserved until the bioglass samples reached room temperature. The surfaces produced in bioglass samples due to electrical polarization were named “P-surface” and “N-surface” for positive and negatively charged surfaces [34]. Figures 7.1(a) and 7.1(b) graphically depict the electrical poling technology in operation. Here, we see the movement of ions within the cathode and anode, as shown in figures after polarization within the charged parallel plates.

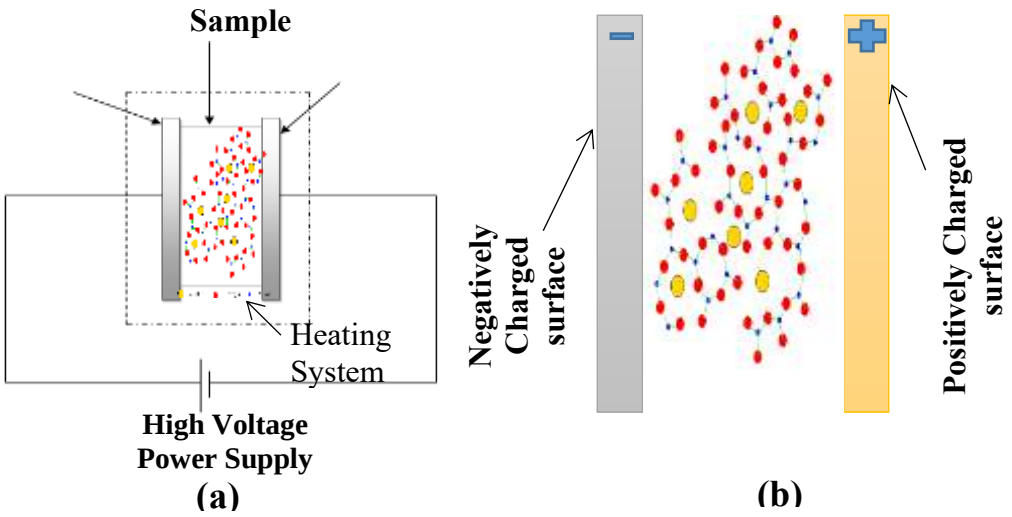

Figure 7.1 (a) Illustration of Electro thermal poling Experiment **(b)** After poling, the negative and positive charged surfaces are designated as "N-Surface" and "P-Surface".

7.3 Result and Discussion

7.3.1 Thermal Properties:

During differential thermal analysis (DTA) ZBG0 sample, two distinct peaks, one endothermic peak at 530ºC and the other exothermic peak at 722ºC, are obtained. They are linked to the glass transition temperature Tg and glass crystallization temperature Tc, respectively, in Figure 7.2(a) [16].

7.3.2 Physical Properties:

The density of the prepared samples was calculated and found to increase with the doping of ZnO, as shown in Figure 7.2(b). Before being submerged in SBF, the ZBG samples' XRD is shown in Figure 7.3. Except for a hump from 25º to 32º, this is caused by the Si-O-Si arrangement. No peak demonstrating the amorphous structure of any sample was identified [19]. Before being immersed in SBF, the ZBG samples' FTIR analysis is shown in Figure 7.4. It displays high peaks in the Si-O stretching (914 cm-1), Si-O-Si bending (450 cm-1), and Si-O-Si (tetrahedral) bands [23], which are well-acknowledged to be the critical characteristics of silicate networks [22]. There are more bonds except Si-O-Si, like phosphate Ca-O group, and in the case of zinc doping, ZnO bonds may be present in SEM and EDS explanation.

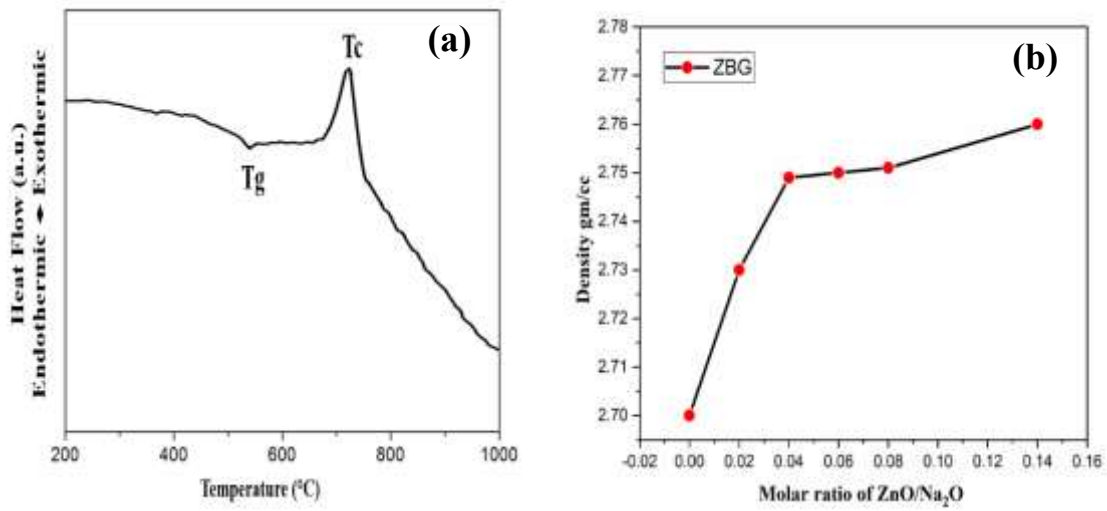

Figure 7.2 (a) DTA value **(b)** Density of base, and ZnO substituted 45S5 bioglass samples.

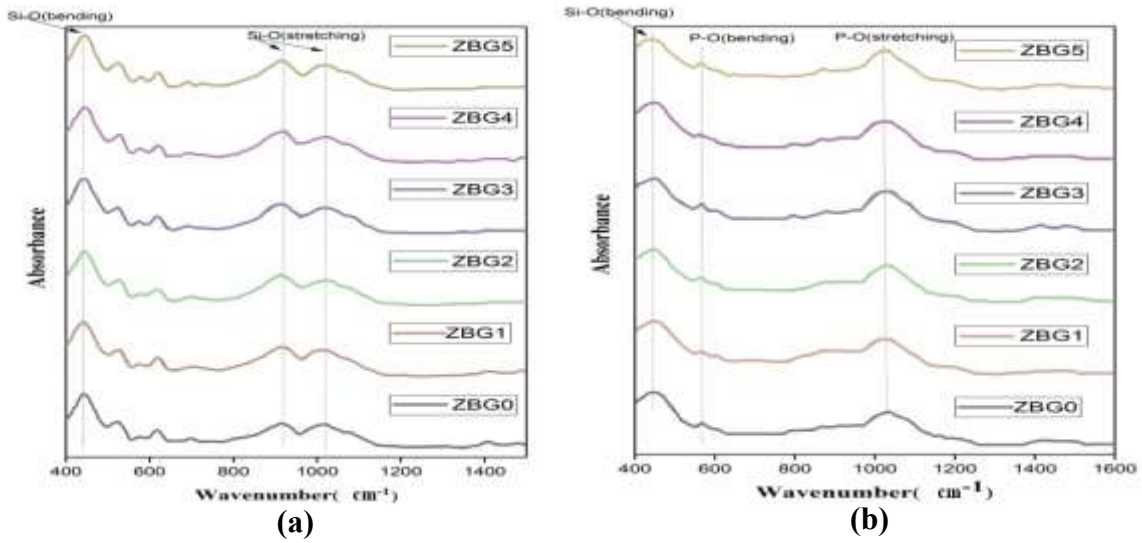

Figure 7.3 FTIR of ZnO substituted 45S5 bioglass **(a)** before immersion in SBF **(b)** after 15 days of immersion in SBF solution.

7.3.3 *In-vitro* bioactivity analysis

The *in-vitro* biological activity was analyzed through the formation of a hydroxyl apatite layer after immersion in an SBF solution. The exchange of ions between the sample surface and SBF solution ions leads to apatite formation, which connects bone to tissues. The effect of ZnO substitution and electrical poling on apatite formation when submerged in SBF was characterized by FTIR, XRD, SEM-EDS, and AFM analysis processes.

7.3.3.1 FTIR: The presence of the bond in the samples before SBF exposure has been seen in Figure 7.3(a), where only the Si bond is observed. The unpoled bioactive glasses were submersed in SBF solution for 15 days. The FTIR results studied for these are shown in Figure 7.3(b). The presence of the hydroxyapatite layer is suggested by observing P-O linkages at 560 and 1060 cm^{-1}. The discrimination between them becomes challenging because of the expansion of the phosphate bond (P-O bond) at 1060 cm^{-1} wavenumber, which is positioned alongside the elongating Si-O bonds. P-O bending and P-O bond stretching is found in the range 530-630 cm^{-1} and 980-1180 cm^{-1} respectively. The sharpness of peaks increases as the zinc doping is increased in the samples showing more phosphate bond formation.

Consequently, the observed peaks occurring at a wavenumber of 560 cm^{-1} may be credited to the presence of the HCA layer. Significantly, the strength of these peaks exhibits an upward trend in correspondence with the rising zinc concentration. To provide a semi-quantitative assessment of the peak intensity, a calculation was performed to determine the ratio of P-O bond intensity at 560 cm^{-1} related to the Si-O bonding intensity at 460 cm^{-1} [28]. Table 7.2 displays the ratio between the peak intensity of P-O twisting at 560 cm^{-1} and the peak intensity of Si-O bending. The observed increase in apatite layer formation is positively correlated with the rise in zinc content, as shown by the growing intensity ratios [29].

Table 7.2 Absorbance Intensity Ratio of P-O Bending at 560 cm^{-1}over Si-O Bending at 470 cm^{-1}.

Concentration	Intensity Ratio
ZBG 0	0.40(0.08/0.20)
ZBG 1	0.44(0.11/0.25)
ZBG 2	0.45(0.10/0.22)
ZBG 3	0.47(0.10/0.22)
ZBG 4	0.48(0.12/0.25)
ZBG 5	0.56(0.13/0.23)

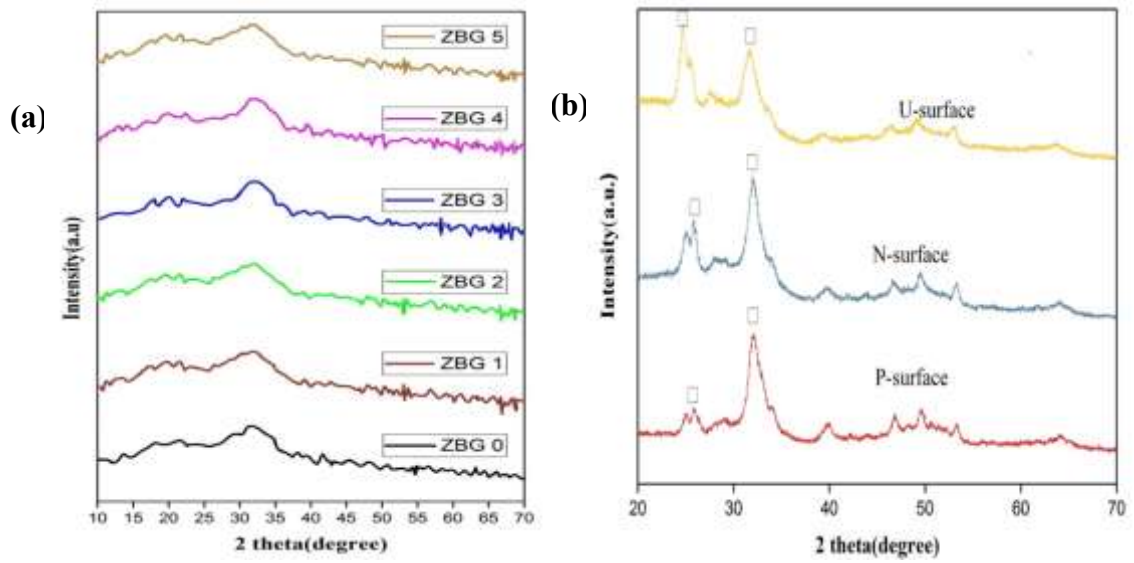

Figure 7.4.1 XRD of **(a)** base and ZnO substituted 45S5 bioglass before immersion in SBF **(b)** unpoled and poled N and P surface after 15 days of immersion in SBF solution.

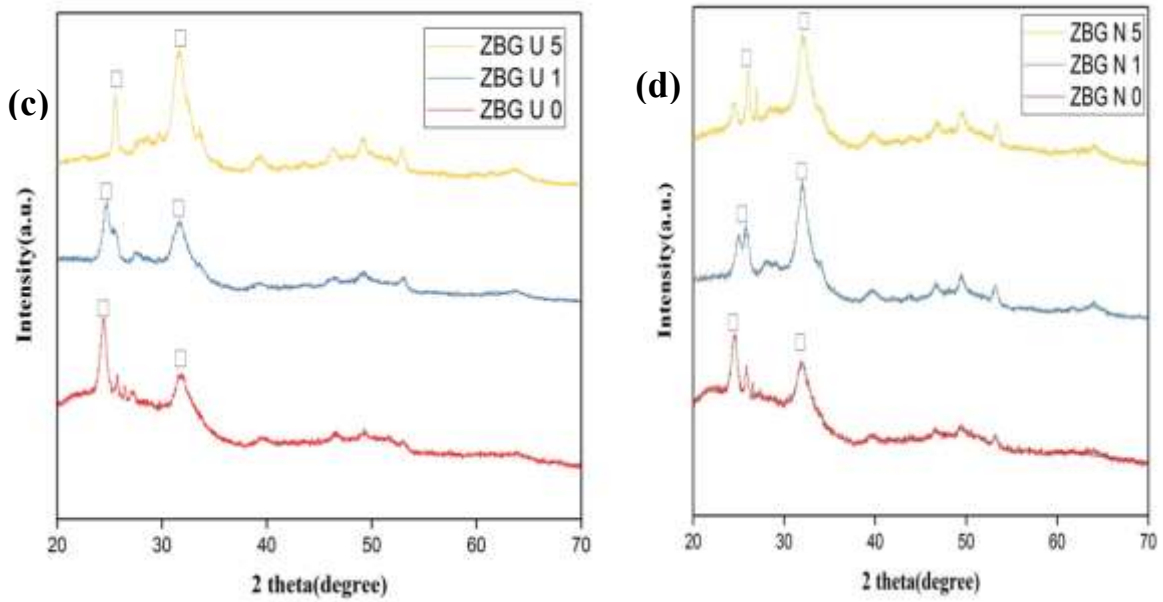

Figure 7.4.2 XRD pattern of **(c)** ZnO substituted 45S5 bioglass Unpoled samples **(d)** Negative charged sample with different concentration after immersion in SBF for 15 days.

7.3.3.2 XRD: Figure 7.4(a) illustrates the XRD pattern of the samples before they were immersed in SBF. Due to the absence of no visible peaks, it is classified as amorphous in nature. Figure 7.4(b) shows the XRD patterns of unpoled, "N-surface," and "P-surface" after 15 days submerged in SBF. The diffraction peaks for the unpoled specimen samples are at 24.5º, and 31.45º corresponds to the formation of HA layers [24]. These peaks could be

identified by their regular JCPDS card number, which was 98-001-2590. In the diffraction pattern of the poled sample labelled as "N-surface" as shown in figure 7.4-b, it was recognized that the higher peak at an angle of 24.5º exhibited higher HCA formation for all samples of zinc bioactive glass (ZBG). It implies that the polling process leads to higher bioactivity because of the higher HCA formation. Additionally, it was observed that the intensity of peaks at an angle of 31.45º increased as the concentration of zinc in the samples increased (figure 7.4-c). However, the intensity of peaks at 24.5º remained relatively constant. Similar to what was shown for unpoled, the intensity of the principal peaks at 31.5º for the polarized sample "N-surface" exhibits a similar pattern (figure 7.4-d). Furthermore, in order to further investigate the effects of poling, we looked at the diffraction patterns of unpoled, "N-surface," and "P-surface" for the ZBG1 and ZBG5 samples (figure 7.4-b). We found that "P-surface" had weaker peaks at 24.5º than "N-surface" alongside unpoled samples, indicating that "P-surface" had less HA formed. [39].

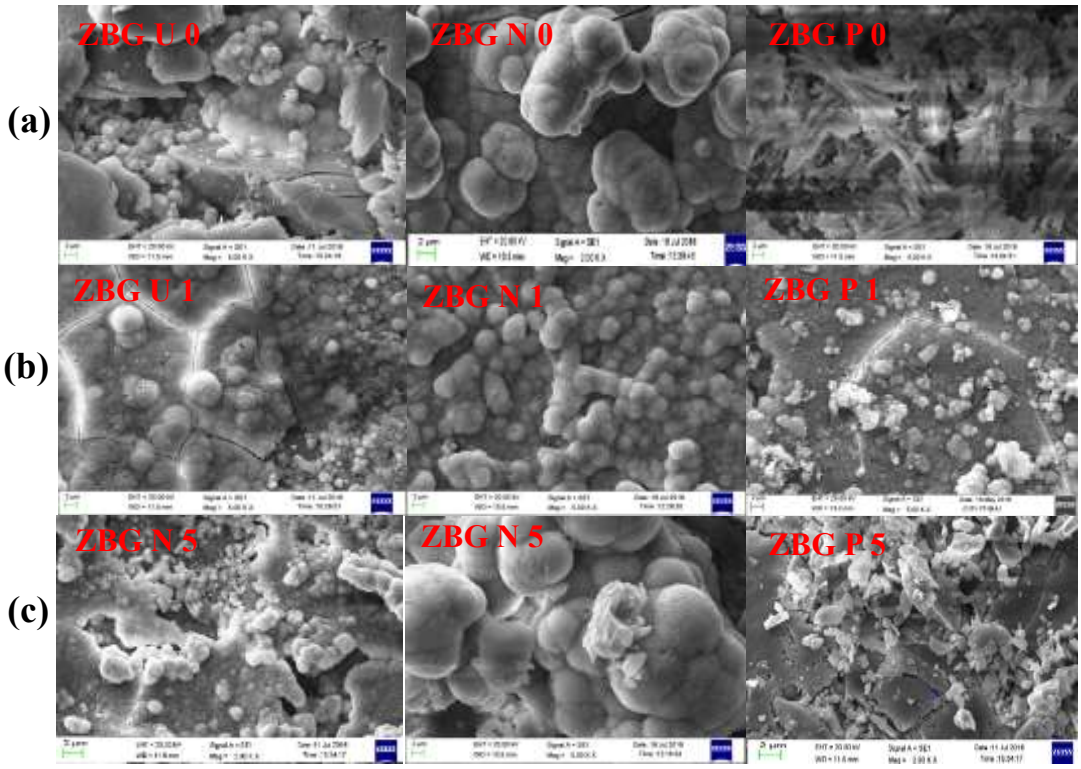

Figure 7.5 SEM images analysis of **(a)** base samples **(b)** 1% mole concentration ZnO substituted samples and **(c)** 3% mole concentration ZnO substituted samples after SBF immersion for unpoled sample, 'N' Surface of polarized sample and 'P' Surface of polarized sample respectively.

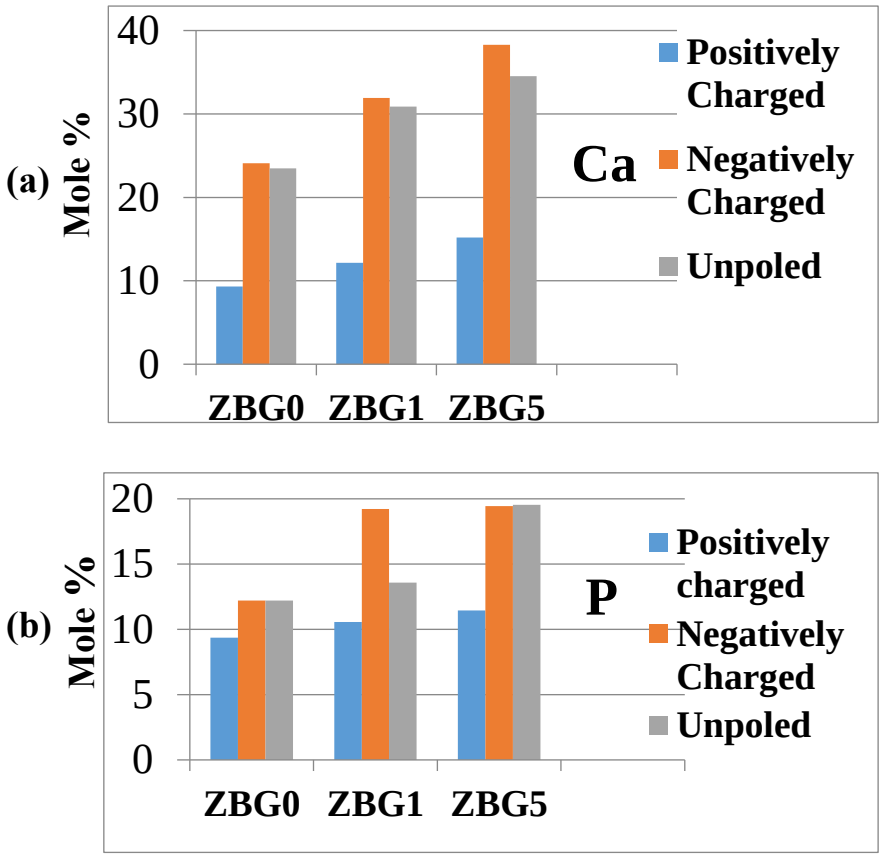

Figure 7.6 EDS analysis of **(a)** Calcium mole concentration **(b)** Phosphorous mole concentration.

7.3.3.3 EDS and SEM analysis: Figure 7.5 shows the surface morphology of 45S5 bioactive glass samples that have been submerged in SBF solution for 15 days for both unpoled and poled (N and P surface) with increasing concentrations of zinc. In Figure 7.5-a, the unpoled samples (ZBG U 0) had many tiny particles resembling spheres on their surface. At the same time, the ZBG N 0 ("N-surface") had bigger round particle sizes that were more noticeable because the sample had been polled. Meanwhile, the ZBG P 0 ("P-surface") samples showed only a negligible development of HA, which had smaller particles. In each of these instances, when the zinc concentration increased, more rounded white particles covered the surface (figure 7.5-b, 7.5-c). A few fractures could be visible on the unpoled ZBG sample's surface, but fewer cracks could be seen on the poled ZBG samples' "N-surface", suggesting that the "N-surface" has more HA production. In contrast, "P-surface" shows lesser HA concentrations. 3% ZnO substituted samples (ZBG N 5) show better bioactivity results. EDS analysis of corresponding SEM images is shown in Figure 7.6 (a, b). It shows how calcium and phosphorus

were analyzed using EDS in the area of the sample surface covered with sphere-like particles. These results indicate that phosphorus and calcium contents were increased as zinc concentration increased and also that poled ZBG samples with a "N-surface" were more likely to contain these elements. These results show the formation of the HA layer so the bioactivity of the sample [36].

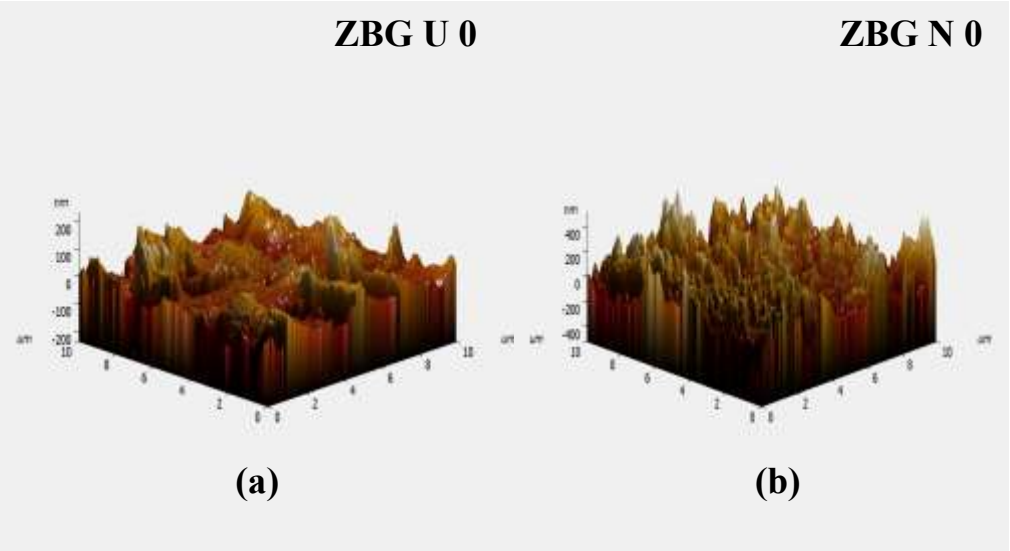

Figure 7.7 AFM analysis of Base sample's surface after SBF immersion **(a)** unpoled sample **(b)** 'N' Surface of polarized sample.

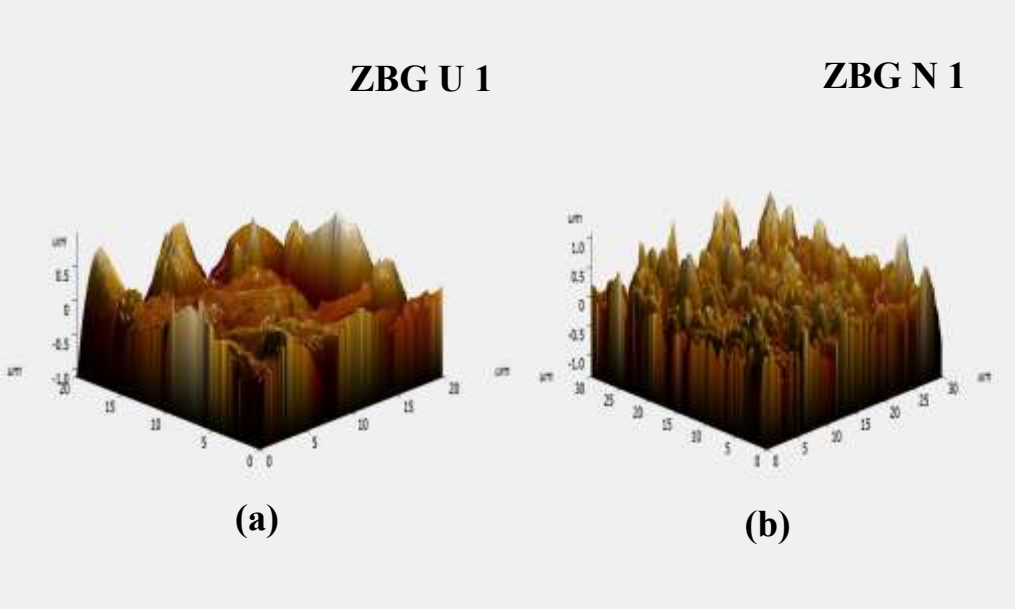

Figure 7.8 AFM analysis of analysis of Zn (1% mole) concentration sample after SBF immersion **(a)** unpoled sample **(b)** 'N' Surface of polarized sample.

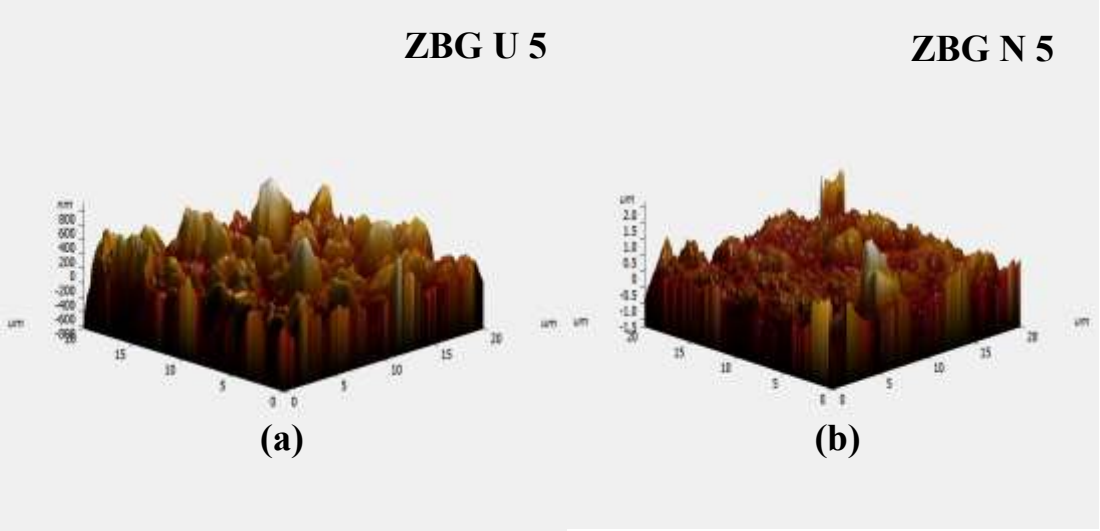

Figure 7.9 AFM analysis of analysis of Zn (5% mole) concentration sample after SBF immersion **(a)** unpoled sample **(b)** 'N' Surface of polarized sample.

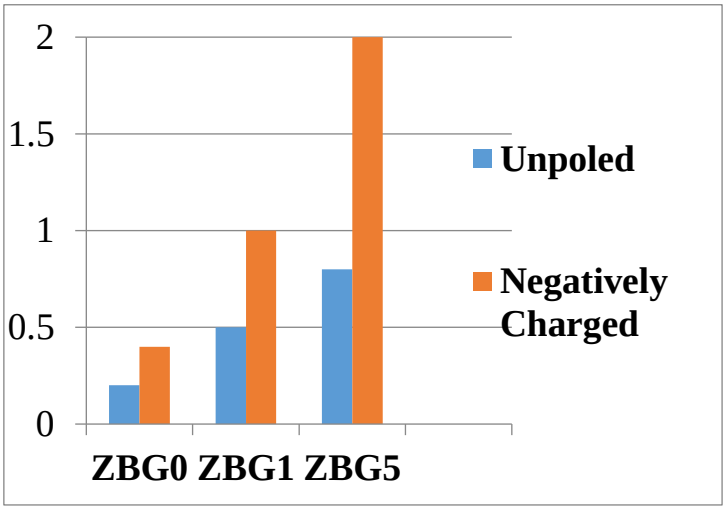

Figure 7.10 AFM results obtained for the samples are displayed in the bar graph.

7.3.3.4 AFM analysis: AFM analysis was used to examine the change in the thickness of produced HA over the ZBG samples after SBF immersion for unpoled (figures 7.7-a, 7.8-a, and 7.9-a) and poled "N-surface" in order to validate the results from XRD, SEM, and EDS. Figures (7.7-b, 7.8-b, and 7.9-b) show the number of islands mounted on the N poled sample, which is higher than the number of islands mounted on the unpoled sample. Figure 7.10 shows how poling increased the height of the island for unpoled and negatively charged samples for different doping arrangements.

There were five different phases that led to the formation of the HA layer on the surface of bioactive glasses, which was a well-known phenomenon. These equations may be used to describe the first two chemical processes. These are:

- Si-O-R (BG) + $H^+ + OH^-$ (SBF) $\longleftrightarrow$ Si-OH + $R^+ + OH^-$……(1)
- The Si-O-Si bond broken while the reaction with OH- ions, leading to formation of Si-O^- and Si-OH bonds instead.
- Si-O-Si + OH^- $\longleftrightarrow$ Si-O^- + Si-OH ……. (2)

  An H_2O molecule interacts with the Si-O- bonds to generate an OH^- ion and another Si-OH, that were free to undergo further reactions (2).
- Si-O^- + $H^+ + OH^-$ $\longleftrightarrow$ OH^- + Si-OH

Electro-poling creates Si-O- and Si-OH groups on the negatively charged surface. This means that putting bioactive glass into SBF creates a negatively charged silica-rich layer on top of the electrically poled N-surface of the bioactive glass. So, this layer takes in Ca^{2+} and P_2O_5 ions from the SBF, which makes solid apatite that looks like bone. We can say that electro-thermal poling changes the bioactivity of 45S5 glass by affecting how fast HA forms and how thick the HA layer is when it comes into acquaintance with SBF.

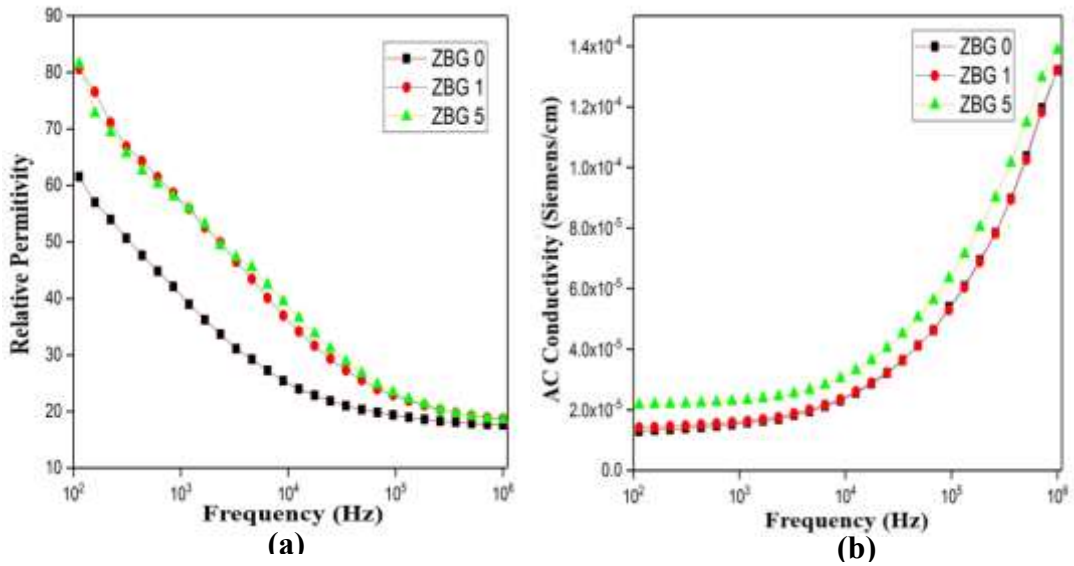

Figure 7.11 (a) Real part of Relative permittivity **(b)** A.C. Conductivity versus Frequency.

Table 7.3 Dielectric constant value of corresponding samples at 1 KHz frequency.

Sample Code	Dielectric constant(at 1 KHz frequency)
ZBG 0	35
ZBG 1	37
ZBG 5	56

7.3.4 Dielectric and AC conductivity analysis

In Figure 7.11(a), the shown graph illustrates the correlation between relative permittivity and frequency. It is seen that all ZBG samples have a certain level of dielectric dispersion at frequencies below 1 kHz. The study demonstrated that the distribution level and dielectric permittivity rises when the concentration of ZnO is increased. Unpolarized zinc bioactive glass (ZBG) samples may exhibit dispersion at low frequencies due to many factors, such as the presence of particle dipole moment and the existence of direct current (dc) conductivity [37]. High dielectricity will enhance the doping of the ZnO due to high permittivity in the parallel plate capacitor model Figure 7.1(a-b). Thus, the higher degree of polarization has resulted in better HCA growth on ZnO-substituted 45S5 bioglass [38].

The accompanying image shows the relationship between frequency and dielectric loss (tan delta), as seen in Table 7.3. The graph shows that the dielectric loss value at frequencies over 1 kHz is below unity. The alternating current (AC) conductivity of the unpoled ZBG samples, evaluated at ambient temperature over various frequencies, shows slight fluctuation with spectrum shift, as seen in Figure 7.11(b). The conductivity has a direct relationship with frequency (f) at higher rates (>1 KHz), displaying power law characteristics [39]. It has been shown that the AC conductivity of the bioactive glass samples increases at a specific frequency with increasing zinc concentrations. Further enhancement in AC conductivity will improve the sample response to the applied electric field. This has resulted in a higher degree of polarization

of the sample during the poling experiment. This phenomenon shows a more significant occurrence of ionic movement when the zinc content is raised by up to 3 mole %. This increase *in-vitro* biological activity may be attributed to the rise in zinc concentration.

7.4. Summary:

The present experimental findings demonstrate the viability of enhancing the bioactivity of bioactive glasses by speeding up the production of HCA by combining the effects of chemical mix modification and electro-thermal poling i.e. the bioactivity of zinc substituted polarized bioactive glasses increased. Density, dielectric property and bioactivity of the produced samples were enhanced with the incorporation of higher levels of zinc, resulting in the substitution of Na_2O with ZnO. Subsequent investigations FTIR, XRD, SEM and EDS have shown that the application of electrical polarization to the N-surface of the bioactive glass samples leads to an augmentation of the HCA layer formation over the ZBG sample. Hence, it can be proven that the use of electrically polarized bioactive 45S5 glass N -surface is a more suitable as compared to its unpolarized counterpart. Thus, these bioactive glasses bind to the host tissue chemically, form a bone-like structure, and have the ability to activate required genes that facilitate osteoblast proliferation and differentiation to promote bone generation quickly. Thus improving the quality of life for human beings and more suitable for medical applications.

References:

[1] L.L. Hench, The story of Bioglass, Journal of Materials Science: Materials in Medicine 17 (2006) 967–978

[2] L.L. Hench, Bioceramics, Journal of the American Ceramic Society, 81 **(**2005) 1705–1728.

[3] P. Ducheyne, Q. Qiu, Bioactive ceramics: the effect of surface reactivity on bone formation and bone cell function, Biomaterials 20 (1999) 2287–2303.

[4] V.K. Vyas, A.S. Kumar, A. Ali, S. Prasad, P. Srivastava, S.P. Mallick, M. Ershad, S.P. Singh, R. Pyare, Assessment of nickel oxide substituted bioactive glass-ceramic on in vitro bioactivity and mechanical properties, Boletín de La Sociedad Española de Cerámica y Vidrio, 55 (2016) 228–238

[5] V.K. Vyas, S.K. Arepalli, S.P. Singh, R. Pyare, Destructive and non-destructive behavior of nickel oxide doped bioactive glass and glass-ceramic, Journal of the Australian Ceramic Society 53 (2017) 939–951.

[6] A.K. Srivastava, R. Pyare, S.P. Singh, In Vitro Bioactivity and Physical–Mechanical Properties of MnO2 Substituted 45S5 Bioactive Glasses and Glass-Ceramics, Journal of Biomaterials and Tissue Engineering, 2 (2012) 249–258.

[7] M.R. Majhi, R. Pyare, S.P. Singh, Preparation and Characterization of CaF2 Doped Bioglass Ceramics, Journal of Biomimetics Biomaterials and Tissue Engineering, 11 (2011) 45–66.

[8] S.K. Arepalli, H. Tripathi, V.K. Vyas, S. Jain, S.K. Suman, R. Pyare, S.P. Singh, Influence of barium substitution on bioactivity, thermal and physico-mechanical properties of bioactive glass, Materials Science and Engineering: C, 49 (2015) 549–559.

[9] V.K. Vyas, A.S. Kumar, S.P. Singh, R. Pyare, Effect of nickel oxide substitution on bioactivity and mechanical properties of bioactive glass, Bulletin of Materials Science, 39 (2016) 1355–1361.

[10] S. Prasad, V.K. Vyas, R. Pyare, K. Mani, Study of physical and mechanical properties of BG/HA/TiO2 biocomposite for bone implantation, International Journal of Advanced Research, 4 (2016) 268–279.

[11] S.K. Yadav, S. Ray, M. Ershad, V.K. Vyas, S. Prasad, A. Ali, S. Yadav, M.R. Majhi, R. Pyare, Development of Zirconia Substituted 1393 Bioactive Glass for Orthopaedic Application, Oriental Journal of Chemistry, 33 (2017) 2720–2730.

[12] S.K. Singh, J. Kumar, P. Singh, S.K. Rajput, A.K. Dubey, R. Pyare, P.K. Roy, Impact of 13-93 bio-glass inclusion on the machinability, in-vitro degradation, and biological behavior of Y-TZP-based bioceramic composite, Ceramic International, 50 (2023) 1087–1106.

[13] M. Ershad, V.K. Vyas, S. Prasad, A. Ali, R. Pyare, Effect of Sm2O3 substitution on mechanical and biological properties of 45S5 bioactive glass, Journal of the Australian Ceramic Society, 54 **(**2018) 621–630.

[14] M. Ershad, V.K. Vyas, S. Prasad, A. Ali, R. Pyare, Synthesis and Characterization of Cerium- and Lanthanum Containing Bioactive Glass, Key Engineering Materials, 751 (2017) 617–628.

[15] A. Ali, M. Ershad, V.K. Vyas, S.K. Hira, P.P. Manna, B.N. Singh, S. Yadav, P. Srivastava, S.P. Singh, R. Pyare, Studies on effect of CuO addition on mechanical properties and in vitro cytocompatibility in 1393 bioactive glass scaffold, Materials Science and Engineering: C, 93 (2018) 341–355.

[16] A.K. Srivastava, R. Pyare, Characterization of ZnO substituted 45S5 Bioactive Glasses and Glass – Ceramics, Journal of Materials Science Research, 1 (2012) 207.

[17] C. Gao, Q. Gao, X. Bao, Y. Li, A. Teramoto, K. Abe, Preparation and In Vitro Bioactivity of Novel Mesoporous Borosilicate Bioactive Glass Nanofibers, Journal of the American Ceramic Society, 94 (2011) 2841–2845.

[18] K. Singh, I. Bala, V. Kumar, Structural, optical and bioactive properties of calcium borosilicate glasses, Ceramics International, 35 (2009) 3401–3406.

[19] X. Yan, X. Huang, C. Yu, H. Deng, Y. Wang, Z. Zhang, S. Qiao, G. Lu, D. Zhao, The in-vitro bioactivity of mesoporous bioactive glasses, Biomaterials, 27 (2006) 3396–3403.

[20] S. Yadav, P. Singh, R. Pyare, Synthesis, characterization, mechanical and biological properties of biocomposite based on zirconia containing 1393 bioactive glass with hydroxyapatite, Ceramics International, 46 (2020) 10442–10451.

[21] S. Yadav, S. Majumdar, A. Akher, S. Krishnamurthy, P. Singh, R. Pyare, In-vitro Analysis of Bioactivity, Hemolysis, and Mechanical Properties of Zn Substituted Calcium Zirconium Silicate (Baghdadite), Ceramics International, 47 (2021) 16037-16053.

[22] J. Serra, P. González, S. Liste, S. Chiussi, B. León, M.P. Amor, H.O. Ylänen, M. Hupa, Influence of the non-bridging oxygen groups on the bioactivity of silicate glasses, Journal of Materials Science: Materials in Medicine, 13 (2002) 1221–1225.

[23] H. Pirayesh, J.A. Nychka, Sol-Gel Synthesis of Bioactive Glass-Ceramic 45S5 and its in vitro Dissolution and Mineralization Behavior, Journal of the American Ceramic Society, 96 (2013) 1643–1650.

[24] A. Singh, P. Goswami, B. Koch, P. Singh, R. Pyare, Study of Human Osteosarcoma Cell Line Growth, Hemocompatibility, In-vitro Analysis and Physical Properties of V2O5 Substituted Borosilicate Glass, Silicon (2024) 1876-9918.

[25] A. Kumar, C.R. Mariappan, A new biocompatible phosphate free mesoporous calcium borosilicate glass-ceramics for medical application, Materials Letters, 305 (2021) 130752.

[26] A. Kumar, A. Mittal, A. Das, D. Sen, C.R. Mariappan, Mesoporous electroactive silver doped calcium borosilicates: Structural, antibacterial and myogenic potential relationship of improved bio-ceramics, Ceramic International, 47 (2021) 3586-3596.

[27] T. Kokubo, H. Kushitani, S. Sakka, T. Kitsugi, T. Yamamuro, Solutions able to reproducein vivo surface-structure changes in bioactive glass-ceramic A-W3, Journal of Biomedical Materials Research 24 (1990) 721–734.

[28] N. Buatip, N. Promsawat, N. Pisitpipathsin, O. Namsar, P. Pawasri, K. Ounsung, K. Phabsimma, S.T. Rattanachan, P. Janphuang, S. Projprapai, Investigation on electrical properties of BCZT ferroelectric ceramics prepared at various sintering conditions, Integrated Ferroelectrics, 187 (2018) 45–52.

[29] R.A. Hill, A. Knoesen, M.A. Mortazavi, Corona poling of nonlinear polymer thin films for electro-optic modulators, Applied Physics Letters, 65 (1994) 1733-1735.

[30] M. Dussauze, F. Evelyne, M. Lahaye, V. Rodriguez, A. Frédéric, Large second-harmonic generation of thermally poled sodium borophosphate glasses, Optics express, 13 (2005) 4064-4069.

[31] M. Qiu, R. Vilaseca, M. Botey, J. Sellares, F. Pi, G. Orriols, Double fitting of Maker fringes to characterize near-surface and bulk second-order nonlinearities in poled silica, Applied Physics Letters, 76 (2000) 3346-3348

[32] S. Devautour, F. Henn, J.C. Giuntini, J.V. Zanchetta, J. Vanderschueren, Discrimination between dipolar and space-charge relaxation by thermally stimulated current spectroscopy: application to several alkali-exchanged mordenites, Journal of Physics D: Applied Physics, 32 (1999) 147.

[33] K. Yamashita, N. Oikawa, T. Umegaki, Acceleration and Deceleration of Bone-Like Crystal Growth on Ceramic Hydroxyapatite by Electric Poling, Chemistry of Materials, 8 (1996) 2697–2700.

[34] A. Obata, S. Nakamura, Y. Moriyoshi, K. Yamashita, Electrical polarization of bioactive glass and assessment of their in vitro apatite deposition, Journal of Biomedical Materials Research, 67 (2003) 413–420.

[35] N. Pisitpipathsin, P. Kantha, W. Leenakul, P. Sriprapha, K. Pengpat, S. Eitssayeam, G. Rujijanagul, Effect of BaZr0.05Ti0.95O3, Addition on Microstructure and Piezoelectric Properties of Hydroxyapatite Bone Advanced Materials Research 506 (2012) 166–169.

[36] N. Pisitpipathsin, P. Kantha, S. Eitsayeam, G. Rujijanakul, R. Guo, A.S. Bhalla, K. Pengpat, Effect of BCZT on Electrical Properties and Bioactivity of 45S5 Bioglass, Integrated Ferroelectrics, 142 (2013) 144–153.

[37] D.P. Almond, C.R. Bowen, D.A.S. Rees, Composite dielectrics and conductors: simulation, characterization and design, Journal of Physics D: Applied Physics, 39 (2006) 1295–1304.

[38] A.K. Jonscher, The ‘universal’ dielectric response, Nature, 267 (1977) 673–679.

[39] C.R. Mariappan, D.M. Yunos, A.R. Boccaccini, B. Roling, Bioactivity of electro-thermally poled bioactive silicate glass, Acta Biomaterialia 5 (2009) 1274–1283.